ORIGINAL PAPER

Numerical modeling of multiphase first-contact miscible flows. Part 1. Analytical Riemann solver

Ruben Juanes · Knut-Andreas Lie

Abstract In this series of two papers, we present a front-tracking method for the numerical simulation of first-contact miscible gas injection processes. The method is developed for constructing very accurate (or even exact) solutions to one-dimensional initial-boundary-value problems in the form of a set of evolving discontinuities. The evolution of the discontinuities is given by analytical solutions to Riemann problems. In this paper, we present the mathematical model of the problem and the complete Riemann solver, that is, the analytical solution to the one-dimensional problem with piecewise constant initial data separated by a single discontinuity, for any left and right states. The Riemann solver presented here is the building block for the front-tracking/streamline method described and applied in the second paper.

1 Introduction

Gas injection is one of the most widely used enhanced oil recovery processes (Stalkup Jr. 1983; Lake 1989; Orr Jr. 2005). The fundamental principle is the development of miscibility between the resident oil phase and the injected gas, in order to enhance the mobility of the hydrocarbon phase and to achieve a high displacement efficiency. In general, miscibility between the oil present in the reservoir and the

R. Juanes (✉)
Department of Civil and Environmental Engineering, Massachusetts Institute of Technology, Building 48, 77 Mass. Ave., Cambridge, MA 02139, USA
e-mail: juanes@mit.edu

K.-A. Lie
SINTEF ICT, Department of Applied Mathematics,
P.O. Box 124 Blindern, Oslo NO-0314, Norway
e-mail: knut-andreas.Lie@sintef.no

injected gas leads to a complex set of interactions described by thermodynamical equilibrium of the system, in which components of the gas dissolve in the oil, and components of the oil transfer to the vapor (Pope 1980; Helfferich 1981; Hirasaki 1981).

In this series of two papers, we restrict our attention to simplified thermodynamical systems that can be approximated by *first-contact miscible* phase behavior. The underlying assumption is that the injection gas (solvent) and the resident oil mix in all proportions to form a single hydrocarbon phase. This scenario is optimal with respect to local displacement efficiency, and can be achieved in practice if the gas is injected at a pressure well above the minimum miscibility pressure (Wang and Orr Jr. 1997; Jessen et al. 1998).

We present a computational framework for the efficient simulation of first-contact miscible processes in three-dimensional, heterogeneous reservoir models. The key ingredients of our approach are:

1. An analytical solution of the one-dimensional Riemann problem for a three-component, two-phase system under the assumption of first-contact miscibility of the hydrocarbon components, assuming that the effects of viscous fingering are negligible.
2. A front-tracking algorithm that makes use of the analytical Riemann solver as a building block for obtaining approximate solutions to general one-dimensional problems.
3. A streamline simulator that decouples the three-dimensional transport equations into a set of one-dimensional problems along streamlines.

In Part 1, we present the mathematical model of the problem and the complete set of analytical solutions to the Riemann problem. In Part 2, we describe the front-tracking algorithm and streamline simulation framework, along with representative numerical examples in one-, two- and three-dimensional problems.

The proposed framework was employed by the authors for the simulation of immiscible three-phase flow (Lie and Juanes 2005; Juanes et al. 2004), and it is extended here to miscible gas injection problems. The applicability of the framework presented here is limited, however, by the assumption that the effects of viscous fingering are not accounted for. New analytical solutions to macroscopic models of viscous fingering for three-component, two-phase flows (Juanes et al. 2005; Juanes and Blunt 2006a, b) may eventually lead to the development of Riemann solvers that incorporate these effects.

The Riemann problem consists in solving a system of conservation laws in an infinite one-dimensional domain, with piecewise constant initial data separated by a single discontinuity. The development of analytical solutions to the Riemann problem of multiphase, multicomponent flow has received considerable attention over the past two decades (see, e.g. Orr Jr. (2005) and the references therein). Riemann solutions have been constructed for two-phase and three-phase systems with complex phase behavior for particular initial and injection conditions. However, the development of complete Riemann solvers is a much more challenging task. A Riemann solver is a mathematical algorithm that provides the solution to the Riemann problem for *any* initial and injection states. A Riemann solver for polymer flooding was originally presented by Isaacson (1980), and then extended to account for adsorption in two-component (Johansen and Winther 1988) and multicomponent systems (Johansen and Winther 1989; Johansen et al. 1989). The principle behind polymer flooding is the

addition of a *water-soluble* polymer to the injected water to *increase* its viscosity and, consequently, the efficiency of a waterflood. We are interested in miscible flooding, where the injected solvent readily mixes with the *oil* in place, and *reduces* the viscosity of the hydrocarbon phase. However, under a proper change of variables, the mathematical structure of the equations is virtually identical to that of polymer flooding. Therefore, we rely heavily on the developments of Isaacson (1980) and Johansen and Winther (1988) when formulating the complete Riemann solver for first-contact miscible flooding. We extend the formulation (slightly) by accounting for the presence of connate water and residual oil. We also pay special attention to the efficient implementation of the analytical solver, because typical applications require the evaluation of hundreds of millions of Riemann problems (Lie and Juanes 2005).

An outline of the paper is as follows. In Sect. 2, we present the mathematical model describing the first-contact miscible system, and introduce the conservation variables employed in characterizing the solution. We comment on the mathematical character of the system of equations, highlighting the fact that it is not strictly hyperbolic. In Sect. 3, we describe the different waves that may be present, and the complete solution to the Riemann problem. In Sect. 4, we gather the main conclusions and anticipate the use of the analytical Riemann solver in the front-tracking/streamline framework described in detail in Part 2 (Juanes and Lie 2006).

2 Mathematical model

2.1 Governing equations

We derive briefly the governing equations for one-dimensional, two-phase, three-component flow in porous media. The three components are referred to as water (w), oil (o) and solvent or gas (g). In what follows, we shall assume that water is immiscible, and forms an aqueous phase (w). We shall also assume that the two hydrocarbon components (oil and solvent) are fully miscible, and form a nonaqueous hydrocarbon phase (h).

The one-dimensional conservation equation for each of the components can be written as:

$$\frac{\partial m_i}{\partial t} + \frac{\partial F_i}{\partial x} = 0, \quad i = w, o, g, \tag{1}$$

where m_i is the mass of component i per unit volume of porous medium, and F_i is the mass flux of that component. The mass densities are expressed in the following form:

$$m_w = \rho_w \phi S_w, \tag{2}$$

$$m_o = \rho_h \phi S_h \chi_o, \tag{3}$$

$$m_g = \rho_h \phi S_h \chi_g, \tag{4}$$

where ρ_α ($\alpha = w, h$) are the densities of each phase, ϕ is the porosity, S_α are the saturations (volume fractions of each phase), and χ_j ($j = o, g$) are the mass fractions of oil and solvent in the hydrocarbon phase. Eqs. (2)–(4) are subject to the following constraints:

$$S_w + S_h \equiv 1, \tag{5}$$

$$\chi_o + \chi_g \equiv 1. \tag{6}$$

The mass flux of each component, assuming that the macroscopic effects of viscous fingering are negligible, is given by

$$F_w = \rho_w \phi v_w, \tag{7}$$

$$F_o = \chi_o \rho_h \phi v_h, \tag{8}$$

$$F_g = \chi_g \rho_h \phi v_h, \tag{9}$$

where v_α are the average velocities of each phase. A constitutive model for the phase velocities is given by the multiphase extension of Darcy's law. Neglecting the effect of gravity and capillary forces, they take the form:

$$v_w = -\frac{k}{\phi} \frac{k_{rw}}{\mu_w} \nabla p, \tag{10}$$

$$v_h = -\frac{k}{\phi} \frac{k_{rh}}{\mu_h} \nabla p, \tag{11}$$

where k is the absolute permeability of the medium, p is the pressure, and $k_{r\alpha}$ and μ_α are the relative permeability and dynamic viscosity of the α-phase, respectively. For the purpose of this paper, we shall assume that relative permeabilities are functions of the phase saturation only.

Using Eqs. (2)–(9) in Eq. (1), and assuming incompressible fluids that do not experience volume change in mixing ($\rho_\alpha = $ const) and rigid medium ($\phi = $ const), the mass conservation equations for all three components are written as

$$\frac{\partial S_w}{\partial t} + \frac{\partial v_w}{\partial x} = 0, \tag{12}$$

$$\frac{\partial((1 - S_w)(1 - \chi_g))}{\partial t} + \frac{\partial((1 - \chi_g)v_h)}{\partial x} = 0, \tag{13}$$

$$\frac{\partial((1 - S_w)\chi_g)}{\partial t} + \frac{\partial(\chi_g v_h)}{\partial x} = 0. \tag{14}$$

Summing Eqs. (12)–(14), we obtain the *pressure equation*:

$$\frac{\partial v_T}{\partial x} = 0, \tag{15}$$

where $v_T := v_w + v_h$ is the total velocity. The pressure equation is an elliptic equation, which dictates that the total velocity is at most a function of time. We introduce the fractional flow functions:

$$f_w := \frac{\lambda_w}{\lambda_T}, \tag{16}$$

$$f_h := \frac{\lambda_h}{\lambda_T}, \tag{17}$$

where $\lambda_\alpha = k_{r\alpha}/\mu_\alpha$ is the relative mobility of the α-phase, and $\lambda_T := \lambda_w + \lambda_h$ is the total mobility. With these definitions, a set of two independent conservation equations is:

$$\frac{\partial S_w}{\partial t} + v_T \frac{\partial f_w}{\partial x} = 0, \tag{18}$$

$$\frac{\partial((1 - S_w)\chi_g)}{\partial t} + v_T \frac{\partial((1 - f_w)\chi_g)}{\partial x} = 0. \tag{19}$$

It proves useful to express the governing equations above in terms of the following *conservation variables:*

$$S \equiv S_w: \quad \text{water saturation,} \tag{20}$$

$$C \equiv (1 - S_w)\chi_g: \quad \text{solvent concentration.} \tag{21}$$

In what follows, we drop the subscript from the solvent mass fraction, $\chi \equiv \chi_g$. We introduce the dimensionless space and time coordinates:

$$x_D := \frac{x}{L}, \qquad t_D := \frac{1}{L}\int_0^t v_T(\tau)\,d\tau.$$

Using these definitions in Eqs. (18)–(19), one arrives at the final form of the conservation equations:

$$\frac{\partial S}{\partial t} + \frac{\partial f}{\partial x} = 0, \tag{22}$$

$$\frac{\partial C}{\partial t} + \frac{\partial}{\partial x}\left(\frac{1-f}{1-S}C\right) = 0, \tag{23}$$

where f denotes the water fractional flow function, and x and t should be understood as their dimensionless counterparts.

To close the mathematical model, we must provide constitutive relations for the hydrocarbon viscosity and the relative permeabilities. The viscosity of the hydrocarbon phase depends on the viscosities of the oil and gas components μ_o and μ_g (taken as constants) and the gas mass fraction χ in the hydrocarbon phase. Since the gas viscosity is lower (usually much lower) than the oil viscosity, the hydrocarbon viscosity is a decreasing function of the gas mass fraction (see Fig. 1).

We assume that the hydrocarbon relative permeability does not depend on the amount of solvent. In particular, this means that the residual hydrocarbon saturation is invariant. Thus, relative permeabilities of the aqueous and hydrocarbon phases are

Fig. 1 Typical dependence of the hydrocarbon viscosity on the solvent mass fraction
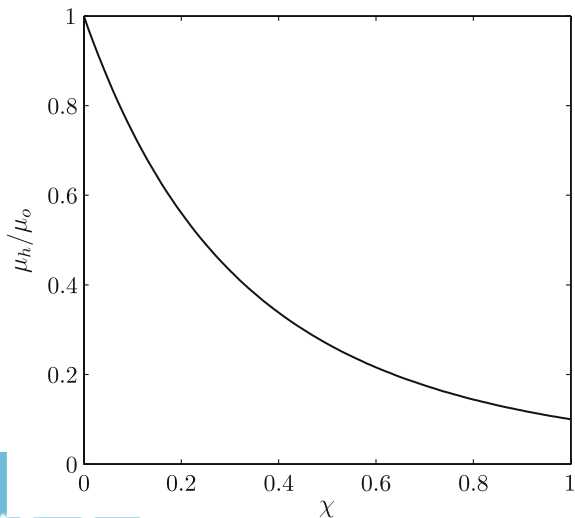
functions of the water saturation only. Typical behavior of these functions is shown in Fig. 2, where we account for the presence of connate water and residual oil. As a result, the fractional flow is a function of both water saturation and solvent concentration:

$$f = \frac{\frac{k_{rw}(S)}{\mu_w}}{\frac{k_{rw}(S)}{\mu_w} + \frac{k_{rh}(S)}{\mu_h(\chi)}} = f(S, C). \tag{24}$$

Since the hydrocarbon viscosity decreases with the solvent fraction, the overall mobility of the hydrocarbon phase is enhanced, resulting in lower values of the water fractional flow. The dependence of the fractional flow function on the solvent mass fraction is illustrated in Fig. 2.

### 2.2 Mathematical character of the equations

We express the system of conservation laws (22)–(23) in vector form:

$$\partial_t \begin{bmatrix} S \\ C \end{bmatrix} + \partial_x \begin{bmatrix} f \\ \frac{1-f}{1-S}C \end{bmatrix} = \begin{bmatrix} 0 \\ 0 \end{bmatrix}. \tag{25}$$

The solution vector (S, C) is restricted to lie on the unit triangle:

$$\mathcal{U} \equiv \{(S, C) : S \geq 0, C \geq 0, S + C \leq 1\}. \tag{26}$$

Fig. 2 Top: relative permeabilities of the water and hydrocarbon phases. Bottom: dependence of the fractional flow function on the solvent mass fraction
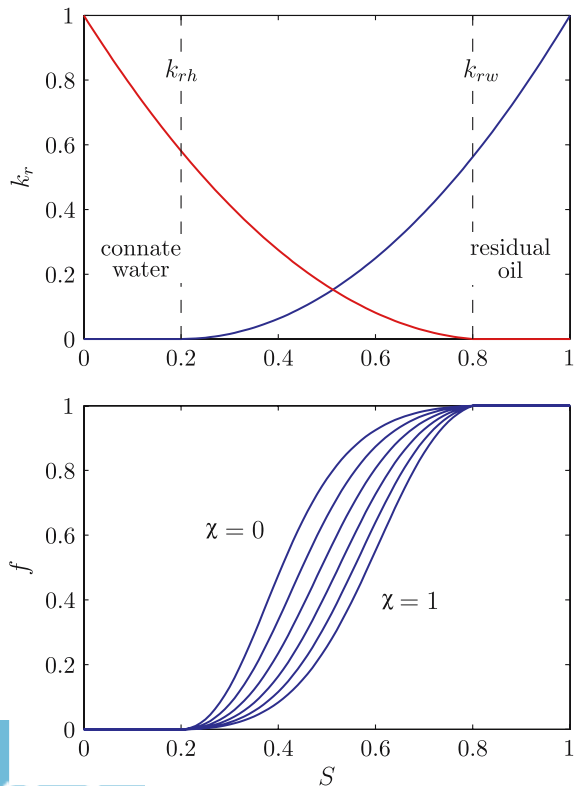
For smooth solutions, the system (25) can be written as

$$\partial_t \begin{bmatrix} S \\ C \end{bmatrix} + A(S,C)\partial_x \begin{bmatrix} S \\ C \end{bmatrix} = \begin{bmatrix} 0 \\ 0 \end{bmatrix}, \tag{27}$$

where A is the Jacobian matrix of the system:

$$A(S,C) := \begin{bmatrix} \frac{\partial f}{\partial S} & \frac{\partial f}{\partial C} \\ \left(\frac{1-f}{1-S} - \frac{\partial f}{\partial S}\right)\frac{C}{1-S} & \frac{1-f}{1-S} - \frac{\partial f}{\partial C}\frac{C}{1-S} \end{bmatrix}. \tag{28}$$

The local character of the system is determined by the eigenvalues and eigenvectors of the Jacobian matrix (Zauderer 1983). The eigenvalues are given by

$$\begin{aligned} v_s = v_s(S,C) &= \frac{\partial f}{\partial S} - \frac{\partial f}{\partial C}\frac{C}{1-S}, \\ v_c = v_c(S,C) &= \frac{1-f}{1-S}, \end{aligned} \tag{29}$$

and the corresponding eigenvectors are:

$$\begin{aligned} r_s &= \begin{bmatrix} 1 \\ -\frac{C}{1-S} \end{bmatrix}, \\ r_c &= \begin{bmatrix} \frac{\partial f}{\partial C} \\ \frac{1-f}{1-S} - \frac{\partial f}{\partial S} \end{bmatrix}. \end{aligned} \tag{30}$$

The eigenvalues v_s and v_c are the characteristic speeds of propagation of waves of the S- and C-family, respectively. The system is hyperbolic if the eigenvalues are real, and strictly hyperbolic if the eigenvalues are real and distinct. In the latter case, the matrix is diagonalizable and there exist two real and linearly independent eigenvectors. If the two eigenvalues are complex conjugates, the system is said to be elliptic.

It is easy to show that the system (25) is hyperbolic, but not everywhere strictly hyperbolic. Loss of strict hyperbolicity occurs in two regions of the composition triangle. First, in the region of residual oil, both eigenvalues are identically equal to zero. The Jacobian matrix is the zero matrix, and every direction is characteristic. Second, there is a curve in phase space at which the eigenvalues coincide, $v_s = v_c$. This curve divides the unit triangle $\mathcal{U}$ into two regions:

$$\begin{aligned} \mathcal{L} &\equiv \{(S,C) : v_s < v_c\}, \\ \mathcal{R} &\equiv \{(S,C) : v_s > v_c\}. \end{aligned} \tag{31}$$

We denote this curve as the *transition curve* $\mathcal{T}$ because the two families of eigenvalues change order as $\mathcal{T}$ is crossed. The regions $\mathcal{L}$ and $\mathcal{R}$ and the transition curve $\mathcal{T}$ are shown on the ternary diagram in Fig. 3. Since the fractional flow function is monotonic with respect to the solvent mass fraction χ, the transition curve intersects each line $\chi = \text{const}$ at exactly one point.

For the first-contact miscible model considered in this paper, the Jacobian matrix is not diagonalizable on $\mathcal{T}$, that is, A has only one independent eigenvector:

$$r_s\big|_{\mathcal{T}} = r_c\big|_{\mathcal{T}} = \begin{bmatrix} 1 \\ -\frac{C}{1-S} \end{bmatrix}. \tag{32}$$

The system is said to have a parabolic degeneracy on $\mathcal{T}$. This behavior is qualitatively very different from that of a model that assumes constant hydrocarbon viscosity. In
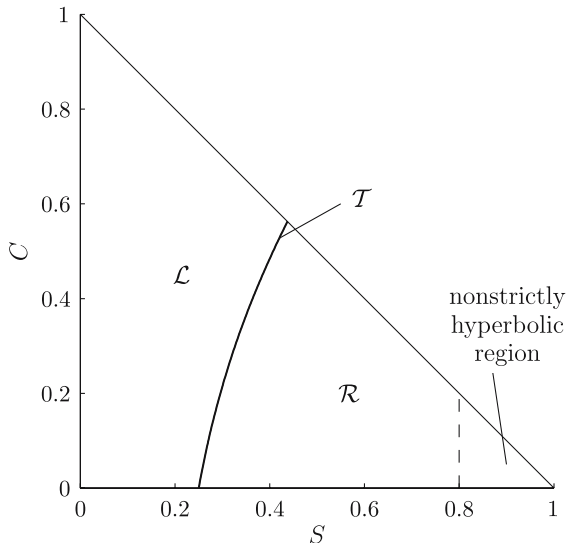
such model, because the fractional flow f is a function of S only, the system is a multiple
of the identity along the transition curve, and every direction is characteristic.

3 The Riemann problem

The Riemann problem consists in finding the weak solution to the system of hyperbolic
conservation laws:

$$\partial_t u + \partial_x F = 0, \quad -\infty < x < \infty, \; t > 0, \tag{33}$$

with the following initial conditions:

$$u(x,0) = \begin{cases} u_l & \text{if } x < 0, \\ u_r & \text{if } x \geq 0. \end{cases} \tag{34}$$

The state $u_l = (S_l, C_l)$ is the 'left' or 'injected' state, and $u_r = (S_r, C_r)$ is the 'right' or
'initial' state. The system of equations (33) and the initial condition (34) are invariant
under uniform stretching of coordinates $(x,t) \mapsto (cx, ct)$. The solution must consist
of centered waves emanating from the origin $(x,t) = (0,0)$. Therefore, we seek a
self-similar solution

$$u(x,t) = U(\zeta), \tag{35}$$

where the similarity variable is $\zeta = x/t$.

3.1 Wave types

In this section, we describe the types of centered waves that arise in the solution of
the Riemann problem of miscible three-component flow.

3.1.1 Integral curves and Hugoniot locus

If the solution $U(\zeta)$ is smooth, it must satisfy

$$A(U)U' = \zeta U', \tag{36}$$

that is, ζ is an eigenvalue and U' is the corresponding eigenvector. Therefore, smooth waves (rarefactions) must lie on an integral curve of the right eigenvectors. States U along an integral curve are defined by the differential equation

$$\frac{dU}{d\tau} = r_i(U(\tau)), \quad i = s, c. \tag{37}$$

Performing the integration analytically, the two families of integral curves are given by the equations:

$$\begin{aligned} S\text{-family}: & \quad \frac{C}{1-S} = \text{const}, \\ C\text{-family}: & \quad v_c = \text{const}. \end{aligned} \tag{38}$$

The derivation of the equation for the S-family curves is obvious from the expression of the corresponding eigenvector r_s in Eq. (30). The equation for the C-family can be obtained by noting that $\nabla v_c \cdot r_c \equiv 0$, that is, the vector ∇v_c in phase space is everywhere perpendicular to the eigenvector r_c. Therefore, curves of the form $v_c = \text{const}$ must be integral curves of r_c. In the context of compositional displacements, integral curves of the S-family are known as *tie-line* paths, and curves of the C-family are termed *nontie-line paths* (Orr Jr. 2005). The integral curves of the system of interest are shown in Fig. 4.

Discontinuous solutions must satisfy an integral version of the mass conservation equations, known as the Rankine–Hugoniot conditions. The set of states u that can be joined to a reference state $\hat{u}$ by a discontinuity satisfy:

$$F(u) - F(\hat{u}) = \sigma(u - \hat{u}), \tag{39}$$

Fig. 4 Integral curves of the S-family (solid line) and C-family (dashed line) on the ternary diagram. Also shown are the inflection locus of the S-family and the transition curve
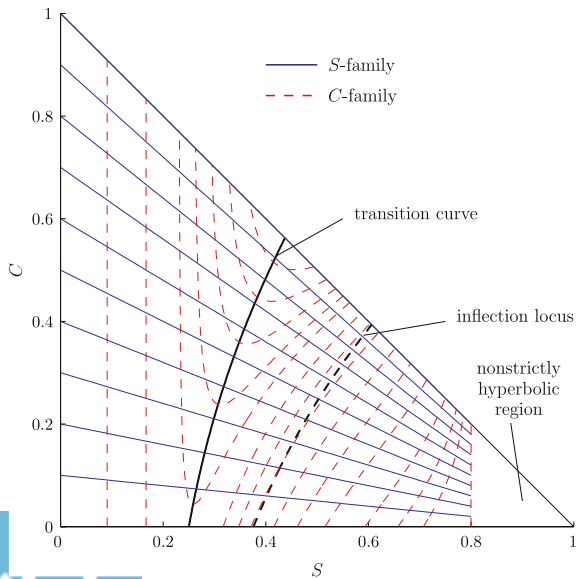
where σ is the speed of propagation of the discontinuity. For the flux vector F of the first-contact miscible problem, Eq. (39) admits two families of solutions, which define the Hugoniot locus of the S- and C-family. In general, integral curves and Hugoniot loci do not coincide, but they have second order tangency (same slope and curvature) at any given state, so they are locally very similar.

The integral curves of the miscible system have the following special features: (1) integral curves of the S-family are straight lines, which means that they have zero curvature; (2) the eigenvalue v_c is constant along integral curves of the C-family, which means that these curves correspond to contact discontinuities. The immediate consequence of these properties is that, for the solvent system, Hugoniot loci and integral curves *coincide*.

Not all states in the Hugoniot locus can be joined to the reference state through a physically admissible discontinuity. A shock must satisfy additional entropy conditions to be physically valid. In this work, we find unique solutions to the Riemann problem that satisfy the e-Lax entropy criterion (Lax 1957; Liu 1974). Therefore, a valid discontinuity that joins states u and $\hat{u}$ may be a *1-Lax shock* if it satisfies:

$$\begin{aligned} v_1(u) \geq \sigma \geq v_1(\hat{u}), \\ \sigma < v_2(\hat{u}), \end{aligned} \tag{40}$$

or a *2-Lax shock* if it satisfies:

$$\begin{aligned} v_2(u) \geq \sigma \geq v_2(\hat{u}), \\ v_1(u) < \sigma. \end{aligned} \tag{41}$$

In Eqs. (40)–(41), $v_1 = \min(v_s, v_c)$ is the smallest eigenvalue and $v_2 = \max(v_s, v_c)$ is the largest eigenvalue. The ordering depends on the location with respect to the transition curve.

3.1.2 Waves of the S-family (Tie-line waves)

Waves of the S-family are solutions of the classical Buckley–Leverett equation. The wave curves are straight lines on composition space, corresponding to lines of constant solvent mass fraction

$$\chi = \text{const.} \tag{42}$$

The characteristic velocity v_s is not constant along integral curves of the S-family. Let us define

$$V_s(u) := \nabla v_s(u) \cdot r_s(u). \tag{43}$$

Since the convexity function V_s changes sign, the S-field is a nongenuinely nonlinear field in the sense of Lax (1957). The *inflection locus* is the set of states where $V_s = 0$, which separates regions of different convexity (see Fig. 4). In our model, the fractional flow function is S-shaped, so the inflection locus intersects each tie-line at exactly one point, which corresponds to a *maximum* of the eigenvalue v_s. It can be shown that, under these conditions, a S-wave can only be of three types: rarefaction, shock, and rarefaction-shock (Ancona and Marson 2001). The admissibility of a S-wave is based on the e-Lax entropy condition (convex-hull construction) (Oleinik 1957; Liu 1974). A robust and efficient algorithm for the determination of the wave structure in the Buckley–Leverett problem is presented elsewhere (Juanes 2005).

3.1.3 Waves of the C-family (Nontie-line waves)

The characteristic speed v_c is constant along wave curves of the C-family. The C-field is a linearly degenerate field in the sense of Lax (1957), and the waves of this family are contact discontinuities. The immediate computational benefit of this property is that evaluation of nontie-line paths does not require numerical integration of an ordinary differential equation: the C-waves are completely determined by the algebraic relation

$$v_c = \text{const.} \tag{44}$$

Application of the e-Lax entropy condition (Liu 1974) precludes the possibility that a C-wave joins constant states on opposite sides of the transition curve (Isaacson 1980).

3.2 Admissible wave sequences

In general, the solution to the Riemann problem consists of a sequence of the centered waves described in the previous section. Before describing the complete solution, we give the admissible sequences of waves that may be present.

3.2.1 The case $u_l \xrightarrow{\mathcal{C}} u_m \xrightarrow{\mathcal{S}} u_r$

Adapting the analysis of Isaacson (1980) to our model problem, it can be shown that the sequence of waves $u_l \xrightarrow{\mathcal{C}} u_m \xrightarrow{\mathcal{S}} u_r$, that is, the combination of a slower C-wave with a faster S-wave, is admissible only in the following three cases:

(a) If $u_m \in \mathcal{T}$ and $u_r \in \mathcal{R}$.
(b) If $u_m \in \mathcal{R}$ and $u_r \in \mathcal{R}$.
(c) If $u_m \in \mathcal{R}$ and $u_r \in \mathcal{L}$ such that $v_c(u_r) \geq v_c(u_m)$.

Examples of each of these wave sequences are given in Fig. 5. The top row of figures show admissible sequences of wave curves in composition space. The bottom row of figures show the fractional flow curve corresponding to the tie-line passing through the intermediate state u_m. In all three cases, the characteristic speed of the C-wave (slope of the dashed line) is less than the characteristic speed of the S-wave (slope of the solid line), indicating admissibility of the wave sequence. In Case (a), u_m is *not* a true intermediate constant state, as the speed of both waves are equal at that point. Therefore, the sequence $\mathcal{CS}$ is in fact a single, coherent wave group.

3.2.2 The case $u_l \xrightarrow{\mathcal{S}} u_m \xrightarrow{\mathcal{C}} u_r$

Similarly, it can be shown that the sequence of waves $u_l \xrightarrow{\mathcal{S}} u_m \xrightarrow{\mathcal{C}} u_r$, that is, the combination of a slower S-wave with a faster C-wave, is admissible only in the following three cases:

(a) If $u_m \in \mathcal{T}$ and $u_l \in \mathcal{L}$.
(b) If $u_m \in \mathcal{L}$ and $u_l \in \mathcal{L}$.
(c) If $u_m \in \mathcal{L}$ and $u_l \in \mathcal{R}$ such that $v_c(u_l) \geq v_c(u_m)$.

In Fig. 6, we show examples of each of these wave pairs, illustrating the sequence of wave curves on the composition diagram and the fractional flow curve of the tie-line
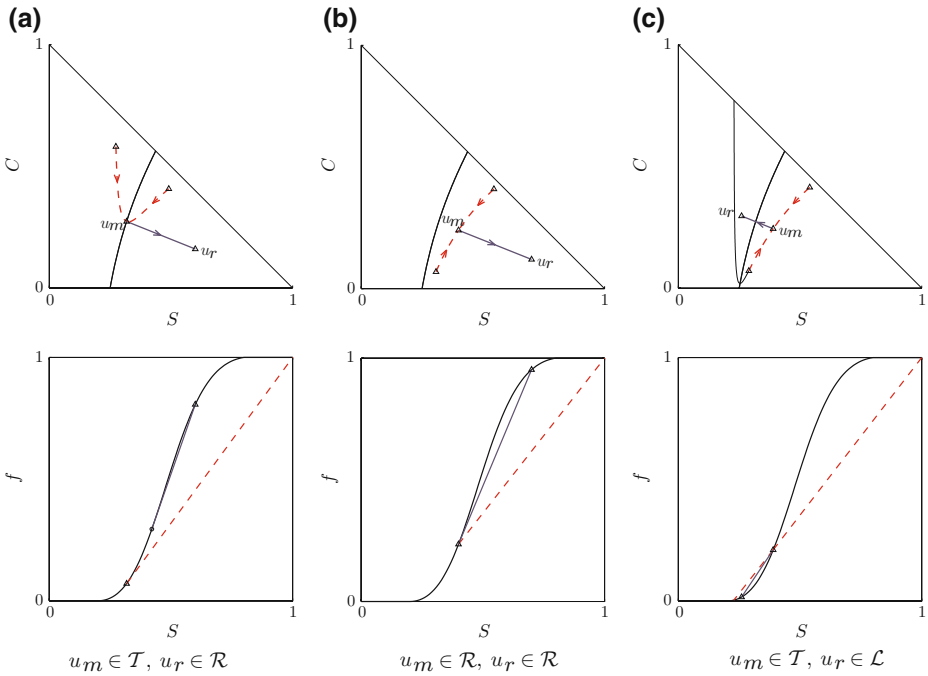
Fig. 5 All three types of compatible wave sequences of type $u_l \xrightarrow{\mathcal{C}} u_m \xrightarrow{\mathcal{S}} u_r$

passing through u_m. Once again, Case (a) corresponds to a single, coherent wave group, in which the C-wave and the S-wave join with equal speeds, and the state u_m in *not* an intermediate constant state.

3.3 Solution of the Riemann problem

The global solution of the Riemann problem is obtained by joining waves that form a compatible sequence. Motivated by the admissible wave structure of Cases 1 and 2 above, and following Isaacson (1980), we define several regions in the composition diagram that will allow a straightforward characterization of the wave structure of the solution.

– The case $u_l \in \mathcal{L}$ (Fig. 7a): One must first identify the tie-line $\chi = \chi(u_l)$ associated with the left state, and the intersection u_t of this tie-line and the transition curve $\mathcal{T}$. Then, we define the following three nonoverlapping regions that cover the entire ternary diagram $\mathcal{U}$:

1. Region $\mathcal{L}_1$: It contains the set of states u satisfying $v_s(u) < v_c(u)$ and $v_c(u) < v_c(u_t)$. Therefore, it is bounded from the right by the transition curve $\mathcal{T}$ and the left branch of the nontie-line passing through the intersection point u_t.

2. Region $\mathcal{L}_2$: It contains the set of states u satisfying that $v_s(u) > v_c(u_t)$ and $\chi(u) > \chi(u_t)$. It is bounded from the left by the left branch of the nontie-line passing through u_t and from below by the tie-line passing through u_t.
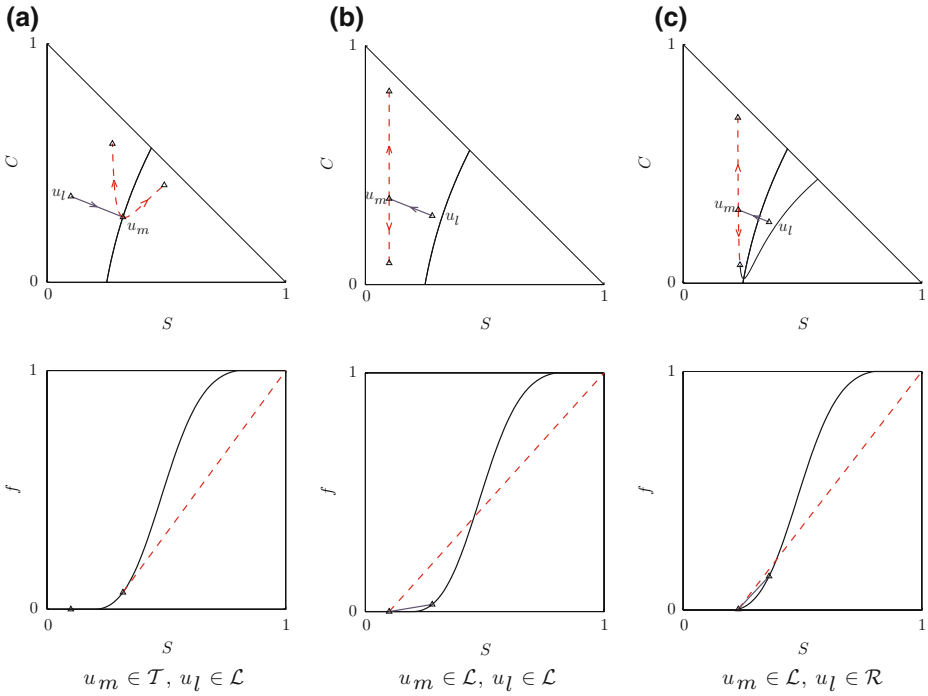
Fig. 6 All three types of compatible wave sequences of type $u_l \xrightarrow{S} u_m \xrightarrow{C} u_r$
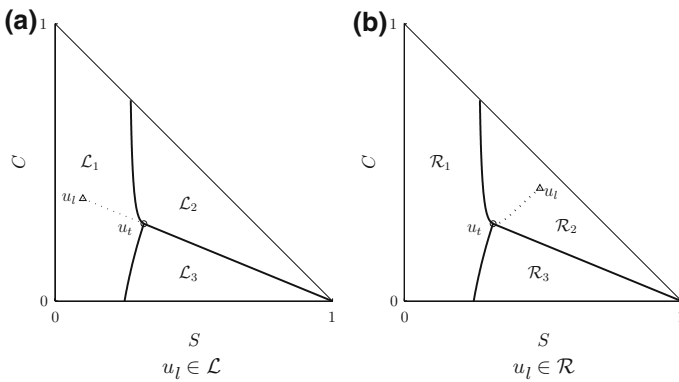

Fig. 7 Regions on the ternary diagram defining the global wave structure of the Riemann solution

3. Region $\mathcal{L}_3$: It contains the set of states u satisfying that $v_s(u) > v_c(u)$ and $\chi(u) < \chi(u_t)$. It is bounded from the left by the transition curve $\mathcal{T}$ and from above by the tie-line passing through u_t.

– The case $u_l \in \mathcal{R}$ (Fig. 7b): We first find the nontie-line $v_c = v_c(u_l)$ associated with the left state, and the intersection u_t of this nontie-line and the transition curve $\mathcal{T}$. It is important to note that this intersection point may be outside the ternary diagram. In that case, some of the regions defined below will be empty:

1. Region $\mathcal{R}_1$: It contains the set of states u satisfying that $v_s(u) < v_c(u)$ and $v_c(u) < v_c(u_t)$. If the intersection point u_t is inside the ternary diagram, this region is bounded from the right by the transition curve $\mathcal{T}$ and the left branch of the nontie-line passing through the intersection point u_t. Otherwise, it is bounded from the right entirely by the left branch of the nontie-line, and it is empty if $v_c(u_l) < 1$.

2. Region $\mathcal{R}_2$: It contains the set of states u satisfying that $v_s(u) > v_c(u_t)$ and $\chi(u) > \chi(u_t)$. If the intersection point u_t is inside the ternary diagram, this region is bounded from the left by the left branch of the nontie-line passing through u_t and from below by the tie-line passing through u_t. If u_t is outside the composition triangle, this region is only bounded from the left by the left branch of the nontie-line $v_c = v_c(u_l)$. If $v_c(u_l) < 1$, this region covers the entire triangle.

3. Region $\mathcal{R}_3$: It contains the set of states u satisfying that $v_s(u) > v_c(u)$ and $\chi(u) < \chi(u_t)$. If the intersection point u_t is inside the ternary diagram, this region is bounded from the left by the transition curve $\mathcal{T}$ and from above by the tie-line passing through u_t; otherwise it is empty.

We are now in position to give the global structure of the solution to the Riemann problem (Isaacson 1980).

– The case $u_l \in \mathcal{L}$ (Fig. 8): If the left state u_l belongs to the region $\mathcal{L}$, that is, if $v_s(u_l) < v_c(u_l)$, the global solution to the Riemann problem is of one of the following types:

1. $u_r \in \mathcal{L}_1$ (Fig. 8(a)): $u_l \xrightarrow{\mathcal{S}} u_m \xrightarrow{\mathcal{C}} u_r$.
2. $u_r \in \mathcal{L}_2$ (Fig. 8(b)): $u_l \xrightarrow{\mathcal{S}} u_t \xrightarrow{\mathcal{C}} u_m \xrightarrow{\mathcal{S}} u_r$.
3. $u_r \in \mathcal{L}_3$ (Fig. 8(c)): $u_l \xrightarrow{\mathcal{S}} u_m \xrightarrow{\mathcal{C}} u_t \xrightarrow{\mathcal{S}} u_r$.

– The case $u_l \in \mathcal{R}$ (Fig. 9): If the left state u_l belongs to the region $\mathcal{R}$, that is, if $v_s(u_l) > v_c(u_l)$, the global solution to the Riemann problem is of one of the following types:

1. $u_r \in \mathcal{R}_1$ (Fig. 9(a)): $u_l \xrightarrow{\mathcal{S}} u_m \xrightarrow{\mathcal{C}} u_r$.
2. $u_r \in \mathcal{R}_2$ (Fig. 9(b)): $u_l \xrightarrow{\mathcal{C}} u_m \xrightarrow{\mathcal{S}} u_r$.

(a)   **(b)**   **(c)**

$u_l \in \mathcal{L}$, $u_r \in \mathcal{L}_1$ $u_l \in \mathcal{L}$, $u_r \in \mathcal{L}_2$ $u_l \in \mathcal{L}$, $u_r \in \mathcal{L}_3$
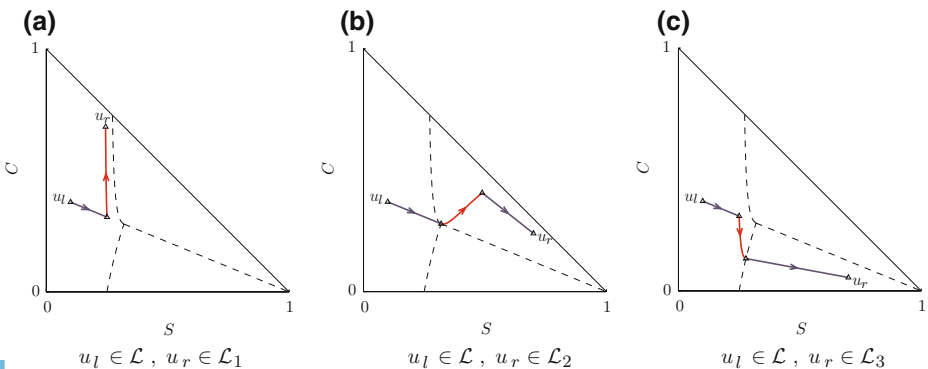
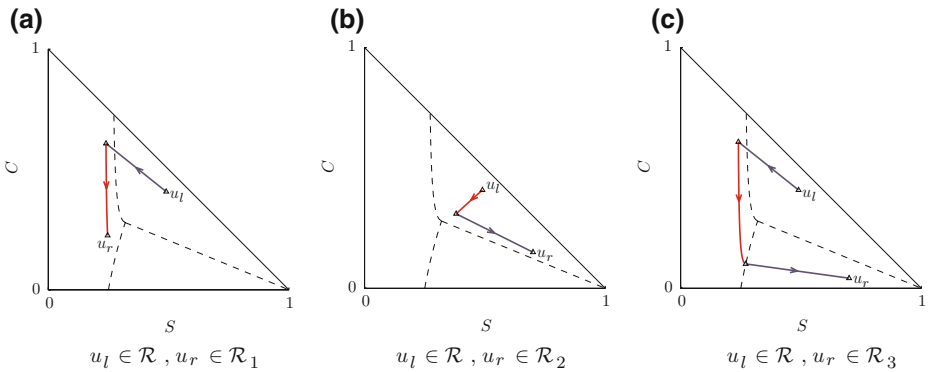**Fig. 8** Wave structure of the solution when $u_l \in \mathcal{L}$

Fig. 9 Wave structure of the solution when $u_l \in \mathcal{R}$

3. $u_r \in \mathcal{R}_3$ (Fig. 9(c)): $u_l \xrightarrow{\mathcal{S}} u_m \xrightarrow{\mathcal{C}} u_t \xrightarrow{\mathcal{S}} u_r$.

The solution to the Riemann problem presented above always exists (by construction) and is the unique solution satisfying the e-Lax entropy criteria (Isaacson 1980). It is important to note that all six solution types are of the form

$$u_l \xrightarrow{\mathcal{W}_1} u_m \xrightarrow{\mathcal{W}_2} u_r, \qquad (45)$$

that is, two wave groups separated by an intermediate constant state. The slow wave $\mathcal{W}_1$ can be of type $\mathcal{S}$, $\mathcal{C}$ or $\mathcal{S}$–$\mathcal{C}$. The fast wave $\mathcal{W}_2$ can be of type $\mathcal{S}$, $\mathcal{C}$ or $\mathcal{C}$–$\mathcal{S}$. Of course, the solution may involve a single wave if the left and right states are on the same tie-line ($u_l \xrightarrow{\mathcal{S}} u_r$) or on the same nontie-line path ($u_l \xrightarrow{\mathcal{C}} u_r$).

3.4 Convergence of finite difference solutions

The purpose of this section is to illustrate the difficulty of standard numerical methods in producing accurate solutions to the Riemann problem. The slow convergence of finite difference solutions to the analytical solution of nonstrictly hyperbolic conservation laws has been noted by many authors (Johansen and Winther 1988; Risebro and Tveito 1991; Jessen et al. 2004). The main reason is the presence of contact discontinuities in the solution. Contact discontinuities are indifferent waves and, unlike genuine shocks, are *not* self-sharpening. As a result, some essential features of the solution may be overwhelmed by numerical diffusion introduced by standard finite difference schemes. High-order finite difference methods—such as total variation diminishing (TVD) schemes (Harten 1983) and Essentially Nonoscillatory (ENO) schemes (Harten et al. 1987)—will generally reproduce contact discontinuities much more accurately, but these methods are more computationally expensive and are less commonly used in reservoir simulation.

Here, we test the performance of two finite volume methods: the standard first-order upwind scheme and a semi-discrete, second-order, central-upwind scheme (Kurganov et al. 2001). In the following, we assume that u_i^n denotes the cell-average function (taken in the componentwise sense):

$$u_i^n := \frac{1}{\Delta x_i} \int_{x_i - \frac{1}{2}\Delta x_i}^{x_i + \frac{1}{2}\Delta x_i} u(x, t^n)\, dx. \tag{46}$$

The upwind scheme has a very simple structure (here $r_i = \Delta t / \Delta x_i$):

$$u_i^{n+1} = u_i^n - r_i\big(F(u_i^m) - F(u_{i-1}^m)\big). \tag{47}$$

Among all conservative first-order, three-point schemes, the upwind scheme is the one with the lowest numerical dissipation and can be used componentwise for the first-contact miscible flow equations, since all eigenvalues of this system are nonnegative. Choosing $m = n$, we obtain an explicit scheme, for which we have the stability requirement that $\max_i v_2(u_i) r_i \leq 1$. A fully implicit scheme is obtained for $m = n + 1$.

The central-upwind scheme is a so-called high-resolution scheme. It generally has five points in the stencil and uses a nonlinear reconstruction to guarantee both second-order accuracy and nonoscillatory behavior. In semi-discrete form, the scheme reads

$$\frac{d}{dt} u_i(t) = H(u_i, t) = -\frac{1}{\Delta x_i}\Big(F_{i+1/2}(t) - F_{i-1/2}(t)\Big). \tag{48}$$

Since all eigenvalues are positive, the numerical flux-functions $F_{i\pm 1/2}(t)$ take a particularly simple form:

$$F_{i+1/2}(t) = F\big(u_i(t) + \tfrac{1}{2}u_i'(t)\big), \tag{49}$$

where $u_i'(t)$ is the *reconstructed* discrete slope,

$$u_i'(t) = L\big(u_i(t) - u_{i-1}(t), u_{i+1}(t) - u_i(t)\big). \tag{50}$$

For the nonlinear limiter function L, we will use the minmod function with $\theta = 1.3$,

$$L(a, b) = \text{minmod}\big(\theta a, \tfrac{1}{2}(a + b), \theta b\big), \tag{51}$$

where

$$\text{minmod}(a, b, c) = \begin{cases} \min(a, b, c), & a, b, c > 0, \\ \max(a, b, c), & a, b, c < 0, \\ 0, & \text{otherwise.} \end{cases} \tag{52}$$

To integrate the semi-discrete equation, we employ a second-order Runge–Kutta scheme based upon combinations of forward-Euler steps:

$$u^{(1)} = u^n + \Delta t^n H(u^n, t^n)$$
$$u^{n+1} = \tfrac{1}{2}u^n + \tfrac{1}{2}\big(u^{(1)} + \Delta t^n H(u^{(1)}, t^n)\big)$$

The stability condition for the central-upwind scheme is $\max_i v_2(u_i) r_i \leq 1/2$.

In Fig. 10, we compare the analytical solution for a Riemann problem of type $\mathcal{R}_3$ with the finite volume solutions at time $t = 0.4$, using two different grids. One of the distinctive features of the solution is the presence of a contact discontinuity of large amplitude, related to the formation of a solvent bank.

The left figures show the comparison with the first-order upwind explicit scheme (Godunov method) using two different grids of 100 and 500 gridblocks. The top figure
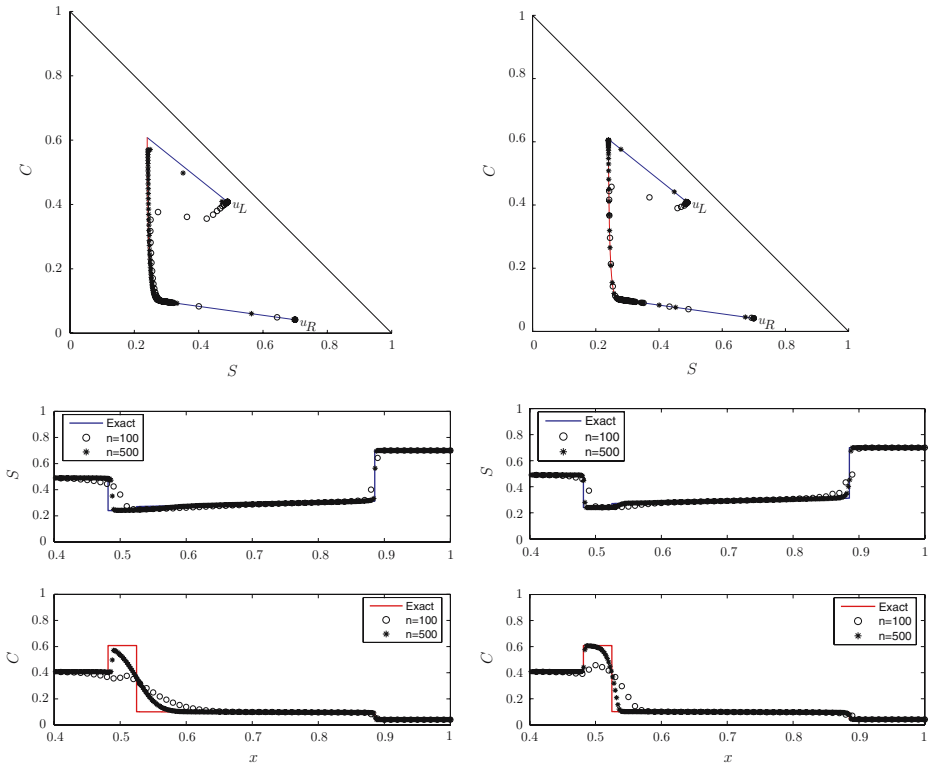
Fig. 10 Comparison between analytical and finite volume solutions for a Riemann problem of type $\mathcal{R}_3$. Left: Numerical solution with the standard upwind explicit method (Godunov method). Right: Numerical solution with the second-order central-upwind method

shows the composition path, and the bottom figures show the profiles of water saturation S and solvent concentration C. It is apparent from the figure that the Godunov method with 100 and 500 gridblocks is unable to resolve solvent bank. The numerical solutions using the second-order TVD scheme are shown on the right. In this case, a grid of 500 elements is sufficient to capture the solvent bank with reasonable accuracy. However, this kind of resolution—500 gridblocks between injection and production wells—is unaffordable in three-dimensional reservoir simulation models.

4 Conclusions

In this paper, we have described a mathematical model and the associated Riemann solver for the simulation of first-contact miscible gas injection processes. Under certain simplifying assumptions, the system describing two-phase, three-component, first-contact miscible flow is a 2×2 hyperbolic system. It is not, however, strictly hyperbolic. Using an analogy with the system of equations governing polymer flooding (Isaacson 1980; Johansen and Winther 1988), we give the complete solution to the Riemann problem.

The efficiency of the front-tracking algorithm to be presented in Part 2 relies heavily on the availability of an analytical Riemann solver. The solvent system studied here has two features that make the front-tracking scheme particularly attractive: (1) rarefaction curves and shock curves coincide in composition space, so there is no need to perform (an expensive) numerical integration to characterize rarefaction waves; (2) some waves are contact discontinuities, which are not self-sharpening. As shown in Sect. 3.4, such waves are very sensitive to numerical diffusion introduced by classical finite difference schemes, but they are resolved *exactly* in a front-tracking solution.

From the point of view of the physical model, the work presented here can be extended in a number of ways. An important extension is to account for viscous fingering. Two of the most commonly used macroscopic models for single-phase miscible displacements are those proposed by Koval (1963) and Todd and Longstaff (1972). Blunt and coworkers proposed an extension of these models to two-phase, three-component, first-contact miscible flows (Blunt and Christie 1993, 1994). Analytical solutions to this model have been developed by Blunt and Christie (1993) and, recently, by Juanes and Blunt (2005, 2006a, b). These new solutions may eventually lead to the development of a full Riemann solver for multiphase first-contact miscible flow models that account for the macroscopic effect of viscous fingering. Another interesting but challenging extension would be to consider multicontact miscible problems, in which the hydrocarbon components do *not* mix in all proportions. Analytical solutions for particular initial and injection states have been presented recently by LaForce and Johns (2005a, b).

The use of the analytical Riemann solver in the context of front-tracking/streamline simulation is the subject of the second paper in this series (Juanes and Lie 2006).

References

Ancona, F., Marson, A.: A note on the Riemann problem for general $n \times n$ conservation laws. J. Math. Anal. Appl. **260**, 279–293 (2001)

Blunt, M., Christie, M.: How to predict viscous fingering in three component flow. Transp. Porous Media **12**, 207–236 (1993)

Blunt, M., Christie, M.: Theory of viscous fingering in two phase, three component flow. SPE Adv. Technol. Ser. **2**(2), 52–60 (1994)

Harten, A.: High resolution schemes for hyperbolic conservation laws. J. Comput. Phys. **49**(3), 357–393 (1983)

Harten, A., Engquist, B., Osher, S., Chakravarthy, S.: Uniformly high-order accurate essentially nonoscillatory schemes, III. J. Comput. Phys. **71**, 231–241 (1987)

Helfferich, F.G.: Theory of multicomponent, multiphase displacement in porous media. Soc. Pet. Eng. J. **21**(1), 51–62 (1981) Petrol. Trans. AIME, 271.

Hirasaki, G.J.: Application of the theory of multicomponent, multiphase displacement to three-component, two-phase surfactant flooding. Soc. Pet. Eng. J. **21**(2), 191–204 (1981) Petrol. Trans. AIME, 271.

Isaacson, E.L.: Global solution of a Riemann problem for a non-strictly hyperbolic system of conservation laws arising in enhanced oil recovery. Technical report, The Rockefeller University, New York (1980)

Jessen, K., Michelsen, M.L., Stenby, E.H.: Global approach for calculation of the minimum miscibility pressure. Fluid Phase Equilib. **153**, 251–263 (1998)

Jessen, K., Stenby, E.H., Orr, F.M.: Interplay of phase behavior and numerical dispersion in finite-difference compositional simulation. Soc. Pet. Eng. J. **9**(2), 193–201 (2004)

Johansen, T., Tveito, A., Winther, R.: A Riemann solver for a two-phase multicomponent process. SIAM J. Sci. Comput. **10**(5), 846–879 (1989)

Johansen, T., Winther, R.: The solution of the Riemann problem for a hyperbolic system of conservation laws modeling polymer flooding. SIAM J. Math. Anal. **19**(3), 541–566 (1988)

Johansen, T., Winther, R.: The Riemann problem for multicomponent polymer flooding. SIAM J. Math. Anal. **20**(4), 908–929 (1989)

Juanes, R.: Determination of the wave structure of the three-phase flow Riemann problem. Transp. Porous Media **60**(2), 135–139 (2005)

Juanes, R., Al-Shuraiqi, H.S., Muggeridge, A.H., Grattoni, C.A., Blunt, M.J.: Experimental and numerical validation of an analytical model of viscous fingering in two-phase, three-component flow. J. Fluid Mech. (In Review) (2005)

Juanes, R., Blunt, M.J.: Analytical solutions to multiphase first-contact miscible models with viscous fingering. Transp. Porous Media **64**(3), 339–373 (2006a)

Juanes, R., Blunt, M.J.: Impact of viscous fingering on the prediction of optimum WAG ratio. In: SPE/DOE Symposium on Improved Oil Recovery. Tulsa, OK. (SPE 99721) (2006b)

Juanes, R., Lie, K.-A.: Numerical modeling of multiphase first-contact miscible flows. Part 2. Front-tracking/streamline simulation. Transp. Porous Media (In Review) (2006)

Juanes, R., Lie, K.-A., Kippe, V.: A front-tracking method for hyperbolic three-phase models. In: European Conference on the Mathematics of Oil Recovery, ECMOR IX, vol. 2, paper B025. Cannes, France (2004)

Koval, E.J.: A method for predicting the performance of unstable miscible displacements in heterogeneous media. Soc. Pet. Eng. J. Petrol. Trans. AIME, 219 145–150 (1963)

Kurganov, A., Noelle, S., Petrova, G.: Semi-discrete central-upwind schemes for hyperbolic conservation laws and Hamilton–Jacobi equations. SIAM J. Sci. Comp. **23**, 707–740 (2001)

LaForce, T., Johns, R.T.: Analytical solutions for surfactant-enhanced remediation of nonaqueous phase liquids. Water Resour. Res. **41** (2005a) Art. No. W10420, doi:10.1029/2004WR003862

LaForce, T., Johns, R.T.: Composition routes for three-phase partially miscible flow in ternary systems. Soc. Pet. Eng. J. **10**(2), 161–174 (2005b)

Lake, L.W.: Enhanced Oil Recovery. Englewood Cliffs, NJ: Prentice-Hall (1989)

Lax, P.D.: Hyperbolic systems of conservation laws, II. Commun. Pure Appl. Math. **10**, 537–566 (1957)

Lie, K.-A., Juanes, R.: A front-tracking method for the simulation of three-phase flow in porous media. Comput. Geosci. **9**(1), 29–59 (2005)

Liu, T.-P.: The Riemann problem for general 2×2 conservation laws. Trans. Am. Math. Soc. **199**, 89–112 (1974)

Oleinik, O.A.: Discontinuous solutions of nonlinear differential equations. Usp. Mat. Nauk. (N.S.) **12**, 3–73 (1957) English transl. in Am. Math. Soc. Trans. Ser. 2, **26**, 95–172

Orr Jr., F.M.: Theory of Gas Injection Processes. Stanford University (2005)

Pope, G.A.: The application of fractional flow theory to enhanced oil recovery. Soc. Pet. Eng. J. **20**(3), 191–205 (1980) Petrol. Trans. AIME 269.

Risebro, N.H., Tveito, A.: Front tracking applied to a nonstrictly hyperbolic system of conservation laws. SIAM J. Sci. Stat. Comput. **12**(6), 1401–1419 (1991)

Stalkup Jr., F.I.: Miscible Displacement, vol. 8 of SPE Monograph Series. Dallas, TX: Society of Petroleum Engineers (1983)

Todd, M.R., Longstaff, W.J.: The development, testing and application of a numerical simulator for predicting miscible flood performance. J. Pet. Technol. **7**, 874–882 (1972)

Wang, Y., Orr, Jr., F.M.: Analytical calculation of the minimum miscibility pressure. Fluid Phase Equilib. **139**, 101–124 (1997)

Zauderer, E.: Partial Differential Equations of Applied Mathematics. New York: John Wiley & Sons (1983)